

TWO TYPES OF ERGOSPHERIC JETS FROM ACCRETING BLACK HOLES: THE DICHOTOMY OF FANAROFF-RILEY GALAXIES

HUNG-YI PU¹, KOUICHI HIROTANI², YOSUKE MIZUNO³, AND HSIANG-KUANG CHANG^{1,3}

Draft version February 21, 2022

ABSTRACT

We investigate the extraction of the rotational energy of a black hole under different accreting environment. When the accretion rate is moderate, the accretion disk consists of an outer thin disk and an inner advection-dominated accretion flow. In such a combined disk, the outer thin disk can sustain a magnetic field with moderate strength at the event horizon, leading to the formation of relativistic jets with moderate luminosity and speed via the magnetohydrodynamic Penrose process. When the accretion rate increases enough, on the other hand, the disk becomes geometrically thin near the horizon. In this slim disk, the denser plasmas can sustain a stronger magnetic field than that in a combined disk, leading to the formation of jets with greater luminosity and speed via the Blandford-Znajek process. It is discussed that the former jets are associated with the Fanaroff-Riley (FR) I galaxies and the latter with FR II galaxies.

Subject headings: accretion, accretion disks — black hole physics — Galaxies: active — magnetic fields — MHD

1. INTRODUCTION

Remarkable advances have been made in explaining the observed spectrum of black hole X-ray binaries (BHXBs) and active galactic nuclei (AGNs) with the help of theoretical studies on black hole (BH) accretion disks (Abramowicz et al. 1999; Kato et al. 2008). Current stable BH accretion disk solutions include the advection-dominated accretion flow, or ADAF for short (Narayan & Yi 1994, 1995; Narayan et al. 1997), the thin disk (Shakura & Sunyaev 1973; Novikov & Thorne 1973), and the slim disk (Abramowicz et al. 1988, 2010; Sądowski 2009; Sądowski et al. 2011). The accretion disk type is a function of the dimensionless accretion rate, $\dot{m} \equiv \dot{M}/\dot{M}_{\text{Edd}} = L/L_{\text{Edd}}$, where \dot{M} is the accretion rate, $\dot{M}_{\text{Edd}} = L_{\text{Edd}}/\xi c^2$ is the Eddington accretion rate, L_{Edd} is the Eddington luminosity, ξ is the efficiency ($\xi = 1$ is adopted for later computation) and c is the speed of light. In Table 1 we summarize the properties of the above disk solutions.

The accretion disk solution is also a function of radius (Abramowicz et al. 1995; Chen et al. 1995). A combined disk which consists of an outer thin disk and an inner ADAF has been also proposed to explain observations of BHXBs and AGNs (Narayan et al. 1996; Esin et al. 1997; Fender et al. 2004; Trump et al. 2011). Such disk is expected to be formed before the entire disk transits from an ADAF to a thin disk, because the hot ADAF would cool down from outside. In other words, the transition radius from outer thin disk to inner ADAF solution decreases as the accretion rate increases until the entire disk becomes thin disk (Honma 1996; Kato & Nakamura 1998; Manmoto et al. 2000). For a comprehensive con-

sideration of how accretion disk type varies with \dot{m} , we also include the combined disk in Table 1.

As a pure relativistic effect, the specific angular momentum of a Keplerian rotating object near the BH, ℓ_k , has a local minimum at the radius of the innermost stable circular orbit, R_{ISCO} . The flow geometry near the BH horizon is determined by how the angular momentum distribution of the accretion disk, $\ell(R)$, deviates from the Keplerian values (Abramowicz 1998). If $\ell(R) > \ell_{\text{ms}}$, where ℓ_{ms} is the Keplerian angular momentum at R_{ISCO} , $\ell(R)$ must equal the Keplerian value twice (assuming $\ell(R) = \ell_k$ at R_1 and R_2 , and $R_2 > R_{\text{ISCO}} > R_1$). In this case, a pressure maximum is formed inside the disk (at R_2) and plasmas are "pushed" towards the BH, forming a 'pressure-driven' flow and resulting in a 'disk-like' structure on the equatorial plane near the horizon. On the contrary, if $\ell(R) < \ell_{\text{ms}}$, the sub-Keplerian plasmas fall into the BH because of the nature of their sub-Keplerian angular momentum ('viscous-driven'). The plasmas are able to fall closer to the axis (i.e., higher latitudes of the horizon), forming a 'quasi-spherical' geometry near the horizon. These two kinds of accretion flow geometry near the horizon, *disk-like* and *quasi-spherical*, was first recognized by Abramowicz & Zurek (1981).

Figure 1 schematically depicts the geometric and dynamic properties of different accretion disks and the extraction of the BH rotational energy when different accretion flow geometries near the horizon are realized. If the magnetosphere near the horizon is filled with plasmas, those plasmas can load onto the large-scale field lines and reduce the electromagnetic extraction of the BH energy (Takahashi et al. 1990). In this letter, by assuming that a relativistic jet is launched when the BH energy is extracted outward, we investigate the formation of BH relativistic jets when the BH is surrounded by different type of disks listed in Table 1. This work is an extension of Pu et al. (2012), hereafter PHC, in which the formation of relativistic jets at low accretion rate (e.g. when $\dot{m} \lesssim 0.1$) is considered. It is found that, ergospheric jets can preferentially take place not only when the BH is sur-

¹ Department of Physics, National Tsing Hua University, Hsinchu 30013, Taiwan

² Theoretical Institute for Advanced Research in Astrophysics, Academia Sinica, Institute of Astronomy and Astrophysics, P.O. Box 23-141, Taipei, Taiwan

³ Institute of Astronomy, National Tsing Hua University, Hsinchu 30013, Taiwan

TABLE 1
SUMMARY OF BLACK HOLE DISK PROPERTIES

Disk Type	ADAF ^a	Combined Disk	Thin Disk	Slim Disk
Accretion Rate	$\dot{m} \ll 0.01$	$\dot{m} \lesssim 0.01$	$0.01 \lesssim \dot{m} \lesssim 0.3$	$0.3 \lesssim \dot{m}$
Cooling Process	advection		radiation	advection
Optical Depth	thin		thick	thick
Disk Geometry	thick ($H \sim R$) ^a	outer thin disk + inner ADAF	thin ($H \ll R$)	thick ($H \lesssim R$)
Viscosity ^b	$\alpha \sim 0.1$		$\alpha \sim 0.01$	$\alpha \ll 1$
Infalling Process	viscous-driven ($\ell_{\text{in}} < \ell_{\text{ms}}$) ^c		viscous-driven ($\ell_{\text{in}} \sim \ell_{\text{ms}}$)	pressure-driven ($\ell_{\text{in}} > \ell_{\text{ms}}$)
Flow Geometry near the Horizon ^d	quasi-spherical		quasi-spherical	disk-like

^a H is the disk height and R is the radial distance to the central BH.

^b α is the parameter in α -prescription (Shakura & Sunyaev 1973).

^c ℓ_{in} is the angular momentum of the flow when it falls onto the BH. See also Figure 1.

^d Note that the geometry of the accretion flow *near the horizon* is determined by the ‘infalling process’ (see text), therefore it can be different from the ‘disk geometry’, which describes the geometry of an accretion disk *far from the horizon*. See also Figure 1.

rounded by a *combined disk*, as suggested in PHC, but also when the BH is surrounded by a *slim disk*. We refer the two types of jets as ‘EJC’ and ‘EJS’, respectively (see section 3). We conclude that the characteristic accretion rate of a EJC and a EJS are $\dot{m} < 0.01$ and $\dot{m} > 0.01$, respectively, and that the EJS is in general more powerful and faster than the EJC for the same central BH mass and BH spin. The difference between these two types of jets may result in the observed dichotomy of FR I and FR II galaxies.

2. IDEAL MHD FLOW

In an axis-symmetry and stationary BH magnetosphere, the total energy of the ideal MHD flow, E , is conserved along a specific field line (see, e.g., PHC for details). We can separate E into the plasma part (the first term) and electromagnetic part (the second term),

$$E = -\mu u_t + \frac{\Omega_F}{4\pi\eta} B_\phi, \quad (1)$$

where μ is the relativistic specific enthalpy, u_t is covariant time component of the four-velocity, Ω_F is the angular velocity of the field, $\eta \propto nu^r/B_r$ is the particle flux per unit flux tube, n is the proper number density, u^r is the radial component of the four-velocity and B_ϕ and B_r is the toroidal and radial field observed by distant observer. Similarly, the total outward energy flux \mathcal{E}^r has the plasma part, $\mathcal{E}_{\text{em}}^r$, and the electromagnetic part, $\mathcal{E}_{\text{plasma}}^r$,

$$\mathcal{E}^r = nEu^r = \mathcal{E}_{\text{em}}^r + \mathcal{E}_{\text{plasma}}^r. \quad (2)$$

A plasma is accelerated along the large-scale magnetic field lines inwards (or outwards) if the gravitational force is larger (or less) than the magnetocentrifugal forces. The conservation of \mathcal{E}^r near the separation region, where the magnetocentrifugal forces balance

with the gravitational force, requires the solution of a powerful outflow (i.e. relativistic jet) to that of an inflow with a positive energy flux ($\mathcal{E}^r > 0$). As discussed in §3.6 of PHC, for the inflow, $\mathcal{E}_{\text{em}}^r > 0$ and $\mathcal{E}_{\text{plasma}}^r < 0$ are generally expected; that is, the magnetic field lines contribute to the extraction of the rotational energy of a BH, while the plasma plays an opposite role and reduces the extraction. Therefore, an MHD flow can extract the BH energy (accordingly a *ergospheric jet* is launched), only when the magnetosphere is magnetically dominated, $|\mathcal{E}_{\text{em}}^r| > |\mathcal{E}_{\text{plasma}}^r|$. The extraction of the rotational energy by the MHD flow is described by the ‘MHD Penrose process’ (Takahashi et al. 1990). When $\mathcal{E}_{\text{plasma}}^r$ is negligibly small compared to $\mathcal{E}_{\text{em}}^r$ (i.e., a nearly vacuum environment), the force-free limit becomes a good approximation. The electromagnetic extraction of the rotational energy of a BH (by large-scale, hole-threading field lines) is described by the ‘Blandford-Znajek process’ (Blandford & Znajek 1977).

3. TWO TYPES OF RELATIVISTIC JET

In general, the strength of a large-scale magnetic field strength⁴ can be parameterized by the ratio, ε^2 , of the gravitational binding energy of the disk at radius R to the large-scale magnetic field energy inside R (see also

⁴ We should stress here that the estimation of *large-scale field* should be different from the estimation of the *local field*, which can be computed by the plasma beta and the gas pressure inside the disk. Numerical simulations, e.x. McKinney et al. (2012) and the references therein, show that the accumulated field strength near the BH can even reach to an equipartition level and supports the accretion disk.

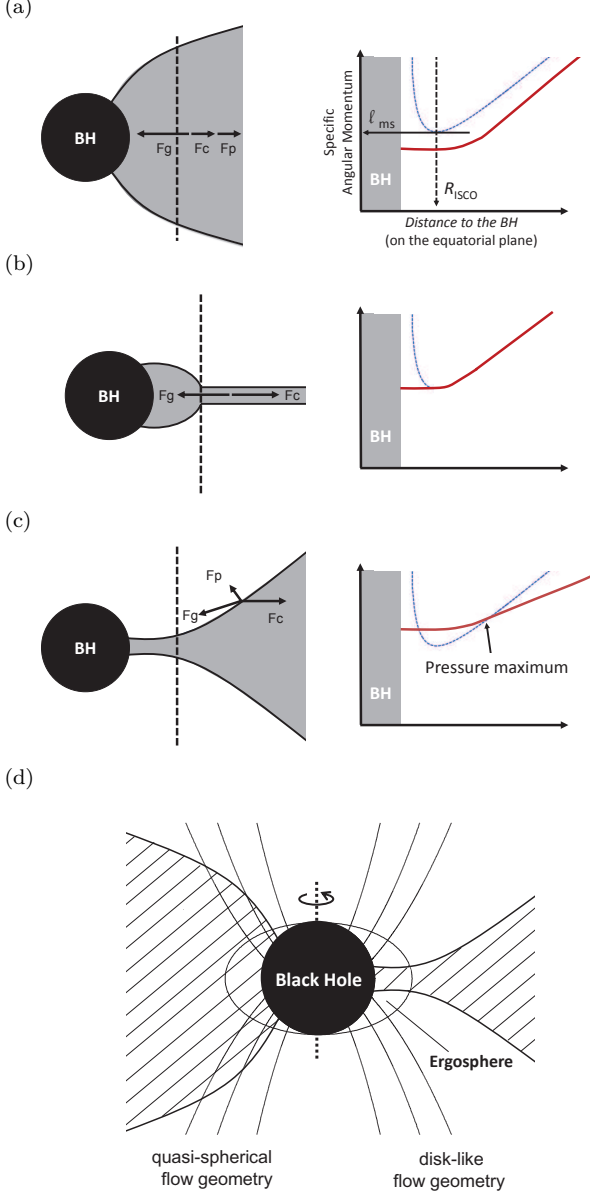


FIG. 1.— (a) Illustration plot (left) and representative angular momentum profile (right) of a ADAF. Dominating forces are shown: F_g , force due to the gravity of the BH; F_c , force due to the rotation of the disk; F_p , force due to the pressure gradient inside the disk. The dashed line represents the location of R_{ISCO} . The specific angular momentum of the disk is shown in red solid curve while the Keplerian value is shown in dashed blue curve. (b) Same as (a), but of a thin disk. (c) Same as (a), but of a slim disk. (d) Extraction of BH rotational energy by a large-scale magnetic field under different accretion flow geometries near the BH horizon (cf. Figure 2 of Abramowicz & Zurek (1981)). The field lines are indicated by solid lines and the accreting plasma are indicated by the shaded region (not to scale). (left) Quasi-spherical flow geometry. Such geometry is resulting from a viscous-driven accretion process, such as an ADAF or a thin disk. The electromagnetic extraction of the BH rotational energy by the field lines is reduced, because the inflowing plasmas along the large-scale field lines bring the rest-mass energies onto the BH. For the thin disk case, the depicted region here is corresponding to a much inner region than R_{ISCO} . (right) Disk-like flow geometry. Such geometry is resulting from a pressure-driven accretion process, such as a slim disk.

PHC). That is,

$$B(\varepsilon, R, \Sigma(R)) = \varepsilon \sqrt{2\pi G M_{BH} \Sigma / R^2}, \quad (3)$$

where G is the gravitational constant and M_{BH} the mass of the central BH. When $\varepsilon = 1$, B reaches a equipartition value at the radius R .

By examining whether the BH rotational energy can be extracted by the MHD flow via the MHD Penrose process when the BH is surrounded by an ADAF, a combined disk or a thin disk, PHC concluded that the jet is most likely launched when the surrounded disk is of a combined disk type among all the cases. Because the surface density of the outer thin disk is much larger than that of the inner ADAF for a combined disk, the inner ADAF can therefore ‘receive’ more large-scale fields from the outer thin disk than what a single ADAF would capture (see equation [3]). Therefore, the quasi-spherical plasma provided by the inner ADAF of a combined disk can be loaded on relatively stronger field lines. Relativistic jets can be finally initiated when the magnetosphere becomes magnetically dominated. This situation can be realized when the transition radius, R_{tr} , where the outer thin disk transits to the inner ADAF, closes enough to the BH. For the convenience of discussion, hereafter we refer this type of jets as *ergospheric jet from the center of a combined disk (EJC)*.

Ergospheric jet can also be preferentially launched when the BH is surrounded by a slim disk. In this case, plasmas enter the BH through a disk-like structure on the equatorial plane and most of the region near the horizon remains nearly vacuum (Figure 1b). Therefore, the Blandford–Znajek process can efficiently operate. Hereafter we refer this type of jets as *ergospheric jet from the center of a slim disk (EJS)*. The power and the speed of the JEC and the EJS are discussed in what follows.

3.1. Jet Power

The total extracted power from a rotating BH can be computed by $P \equiv \int_{R_H} \mathcal{E}^r dS$, where R_H is the radius of the black hole horizon. Similar to Equation (1), we can further divide the power into the electromagnetic part, P_{em} , and the plasma part, P_{plasma} , that is, $P = P_{em} + P_{plasma}$, where

$$P_{em} \equiv \int_{R_H} \mathcal{E}_{em}^r dS, \quad (4)$$

and

$$P_{plasma} \equiv \int_{R_H} \mathcal{E}_{plasma}^r dS. \quad (5)$$

The mathematical similarity of the idea MHD assumption and the force-free assumption guarantees that P_{em} is identical to the output power of Blandford–Znajek process:

$$P_{em} = \frac{1}{32} \omega_F^2 B_H^2 R_H^2 j^2 c, \quad (6)$$

where $j \equiv J/J_{max} = J/(GM^2/c)$, J the angular momentum of the BH, B_H the large-scale hole-threading field strength, and $\omega_F^2 \equiv \Omega_F(\Omega_H - \Omega_F)/\Omega_H^2$, Ω_H the rotational velocity of the BH. Assuming $\omega_F = 1/2$, which maximize P_{em} , we have,

$$P_{em} = \frac{1}{32} \frac{1}{4} B_H^2 \left[1 + \sqrt{(1-j^2)} \right]^2 \left(\frac{GM_{BH}}{c^2} \right)^2 j^2 c. \quad (7)$$

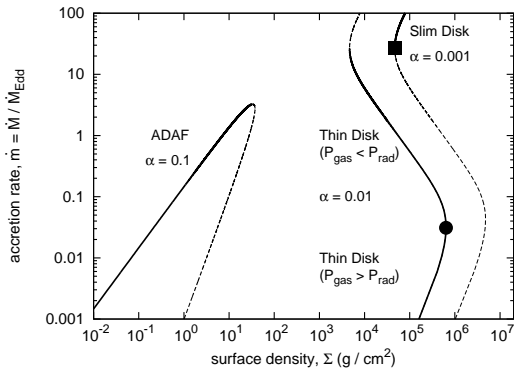


FIG. 2.— Thermal equilibria for accretion disks at $R/R_g = 10$ when $M_{\text{BH}} = 10^9 M_\odot$. The solid curves, from left to right, shows the ADAF solution with $\alpha = 0.1$, thin disk solution with $\alpha = 0.01$ and slim disk solution with $\alpha = 0.001$. The thin disk solution become unstable when the radiation pressure, P_{rad} , dominates the gas pressure, P_{gas} . The filled circle indicates the maximum surface density, Σ , of a thin disk with a fixed α . The maximum Σ is used to evaluate the maximum large-scale field strength that a combined disk can reach (see text for detail). Note that the pseudo-Newtonian potential is adopted here. In a full relativistic computation, the upper turning point of the "S" curve, which is indicated by the filled square and corresponds to the minimum \dot{m} of a slim disk, has a value $\dot{m} \gtrsim 0.3$ (Sądowski 2009; Abramowicz et al. 2010), unlike a large value ($\dot{m} \gg 1$) here.

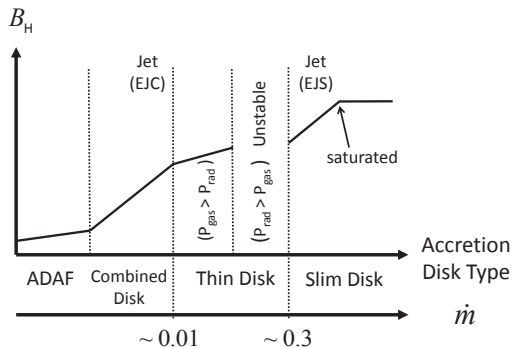


FIG. 3.— Relative large-scale magnetic field strength near the BH, B_H , as a function of the accretion-disk type (or, equivalently, \dot{m}) for a roughly fixed ε , according to Equation (3). The increase of the field strength with increasing \dot{m} in a slim disk levels off at a saturated value. The resulting magnetically dominated magnetosphere when the BH is surrounded by a combined disk or a slim disk, can respectively result in two types of jets, EJC and EJS. See text for more details.

In slim disk case, the accreting plasma, which contributes to P_{plasma} , stay on the equatorial plane. As a result, there is only tiny amount of plasma loading onto the large-scale magnetic field lines that thread the horizon at different latitudes. The jet power of a EJS can be therefore estimated by Equation (7), namely that $P_{\text{EJS}} \approx P_{\text{em}}$. On the other hand, because the plasma with quasi-spherical geometry near the horizon can be loaded onto the field lines and can further reduced the power by the amount of $P_{\text{plasma}} < 0$, Equation (7) represents the *maximum* power of a EJC.

By Equation (3), B_H can be computed if ε and Σ are known. Although the determination of ε is unclear, it should in general has a value $1 > \varepsilon > 0$. Therefore, the changing of B_H at different accretion rate should

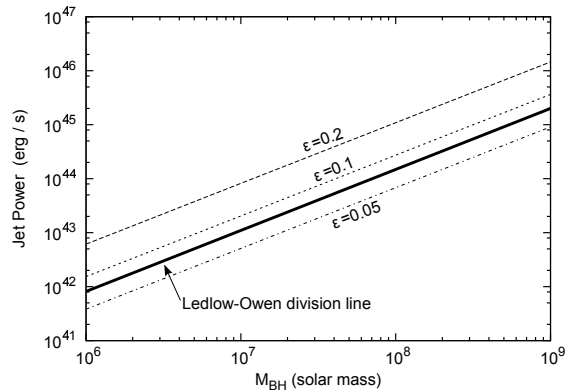


FIG. 4.— Maximum power of the EJC as a function of BH masses with discrete values of ε 's. The long-dashed, short-dashed, and dash-dotted lines represents the case of $\varepsilon = 0.2, 0.1$ and 0.05 , respectively. The power is computed by Equation (5), after the maximum value of B_H is estimated by Equation (3). The spin of the BH, j , is assumed to be 0.6 . Since the mass loading or a smaller spin can further lower the power, the power of EJC will appear in the lower part of these maximum power lines. The FR I/ FR II division line found by Ledlow & Owen (1996) is represented by the solid thick line. Most of FR I (FR II) sources are located above (below) this division line.

mainly be determined by the variation of the surface density of the disk, $\Sigma(\dot{m})$, because it will be higher variable than $\varepsilon(\dot{m})$. Here we assume that the large-scale, disk-threading fields can be dragged inward by accretion flow for *all* types of disks (Narayan et al. 2003; Spruit & Uzdensky 2005; Rothstein & Lovelace 2008) and hence $\varepsilon > 0$ is always satisfied. Note that, in a slim disk, it is the pressure-driven nature (instead of the viscosity) that determines the advection motion of the plasma near the BH. Therefore, although the the magnetic Prandtl number is expected to be small due to a relative tiny value of α compare to other types of disk (Table 1), the field strength near the horizon can be further enhanced when the disk transits from a thin disk to a slim disk, by further pushing a large-scale, disk-threading field lines inward.

Figure 2 presents typical BH accretion disc solution profiles on the $\Sigma - \dot{m}$ plane, following the model in Abramowicz et al. (1995) and Chen et al. (1995). The solid curves represent the solutions of a ADAF, a thin disk and a slim disk with their typical viscosity (see figure caption). With the relation of $\Sigma - \dot{m}$ and Equation (3), relative values of B_H as a function of \dot{m} are qualitatively presented in Figure 3. The field strength gradually increases with increasing \dot{m} when the disk is either an ADAF or a thin disk because of the increase of Σ , where the radiation-pressure dominated thin disk solution is not of interest here because the disk become unstable in that case. For a combined disk, B_H is essentially described by the surface density of the disk at the transition radius, R_{tr} , because the outer thin disk has a much larger density than that of the inner ADAF. The decrease of R_{tr} with increasing \dot{m} results in a rapid growth of B_H with \dot{m} (see also the Figures 1a and 1e of PHC). For a slim disk, although B_H can be further enhanced due to the pushed-in large-scale, disk-threading field lines, the increase of B_H is expected to saturate eventually. This is because the fields diffuse outward outside the pressure-driven region (that is, outside the super-Keplerian part of the disk).

The transition radius of a combined disk continuously decreases with increasing \dot{m} before the entire disk become a thin disk. Previous studies (Honma 1996; Manmoto et al. 2000) show that R_{tr} can reach down to $\sim 10R_g$. For illustration purpose, assuming a modest BH spin, $j = 0.6$, we compute the maximum value of B_H for a combined disk by using the maximum Σ of the (outer) thin disk solution at $R = 10R_g$ (the filled circle in Figure 2) and calculate the resulting *maximum* power of a EJC by equation (3). The jet power for three different ε 's are plotted on the $M_{\text{BH}} - P$ plane (Figure 4). Noting that the plasma contribution, $P_{\text{plasma}} < 0$, as well as a smaller BH spin, will reduce the power of EJC, we find these jet powers represent the upper limits. In other words, the power of a EJC will appear below these lines. On the contrary, for the same parameters (BH mass, BH spin, ε), sources with EJSs will appear above the lines because of a larger B_H (Figure 3) and a negligible P_{plasma} in the force-free limit.

3.2. Jet Speed

By denoting the quantities of the inflow ($u^r < 0$) and outflow ($u^r > 0$) with the subscript "in" and "out", respectively, the ratio of the jet speeds of a EJC and a EJS can be estimated as follows: At large distances, the jet Lorentz factor, Γ , can be defined by

$$\Gamma = \frac{E_{\text{out}}}{\mu}. \quad (8)$$

In addition, near the separation region of the inflow and the outflow, the conservation of \mathcal{E}^r gives,

$$E_{\text{out}} = \frac{n_{\text{in}} u_{\text{in}}^r}{n_{\text{out}} u_{\text{out}}^r} E_{\text{in}}. \quad (9)$$

Thus, for fixed BH mass and spin, the ratio of the power of the EJC and the EJS, χ , can be written as,

$$\chi \equiv \frac{\Gamma^{\text{EJC}}}{\Gamma^{\text{EJS}}} \approx \frac{(n_{\text{out}} u_{\text{out}}^r)^{\text{EJS}}}{(n_{\text{out}} u_{\text{out}}^r)^{\text{EJC}}} \times \frac{(B_r B_\phi)^{\text{EJC}}}{(B_r B_\phi)^{\text{EJS}}}, \quad (10)$$

by the help of Equation (1), where the superscript "EJC" ("EJS") denotes the parameter of EJC (EJS). Because both $(n_{\text{out}} u_{\text{out}}^r)^{\text{EJS}} / (n_{\text{out}} u_{\text{out}}^r)^{\text{EJC}} < 1$ and $(B_r B_\phi)^{\text{EJC}} / (B_r B_\phi)^{\text{EJS}} < 1$ hold, we obtain $\chi \ll 1$.

4. DISCUSSION

The characters of EJC and EJS offer the key to an understanding of the FR I/ FR II dichotomy. The FR I/ FR II division line found by Ledlow & Owen (1996), which is shown by the thick solid line in Figure 4, is roughly consistent with the maximum power that a EJC can reach. It is, therefore, reasonable to suppose that the division reflects the two types of relativistic jets. That is, most FR I (or FR II) galaxies are associated with a EJC (or a EJS). Noting that a EJC has a slower speed than a EJS, why FR I and FR II galaxies have a edge-darken and a edge-brighten morphology, respectively, can be consistently understood as a result of different jet velocities (Bicknell 1985).

Ghisellini & Celotti (2001) found that the accretion rate of FR I and FR II galaxies can be separated at $\dot{m} \approx 0.01$. Similar division of the accretion rates is also indicated for BL Lacs and radio quasars (which are believed to be 'face-on' FR I and FR II galaxies, respectively) (Xu et al. 2009; Ghisellini et al. 2011), and for radio galaxies of 'high-excitation' and 'low-excitation' (Best & Heckman 2012). The corresponding \dot{m} of EJC ($\dot{m} < 0.01$) and EJS ($\dot{m} > 0.01$) are consistent with the above findings.

The major drawback in our calculation is that, the Pseudo-Newtonian potential (Paczynsky & Wiita 1980) is adopted when we use the disk model of Abramowicz et al. (1995) and Chen et al. (1995). We should notice a full-relativistic model (e.g. Sądowski (2009)), could significantly change the range of \dot{m} of the slim disk solution (see captions of Figure 2). Nevertheless, the surface density of the disk solution will not be changed dramatically (Sądowski 2009; Abramowicz et al. 2010; Sądowski et al. 2011). We therefore expect that the results will be qualitatively unchanged when general-relativistic corrections are taken into account. The effect of the BH spin on the jet power, which is beyond the present model, can be investigated in the future by incorporating general relativistic corrections.

H.-Y. thanks Daniel Chun-Cheng Lin for suggestions of figure plotting. This work was supported by the National Science Council (NSC) of Taiwan under the grant NSC 99-2112-M-007-017-MY3, NSC 100-2112-M-007-022-MY3, and the Formosa Program between NSC and Consejo Superior de Investigaciones Científicas in Spain administered under the grant NSC100-2923-M-007-001-MY3.

REFERENCES

- Abramowicz, M. A., & Zurek, W. H. 1981, *ApJ*, 246, 314
 Abramowicz, M. A., Czerny, B., Lasota, J. P., & Szuszkiewicz, E. 1988, *ApJ*, 332, 646
 Abramowicz, M. A., Chen, X., Kato, S., Lasota, J.-P., & Regev, O. 1995, *ApJ*, 438, L37
 Abramowicz, M. A. 1998, in *Theory of black hole accretion discs*, Physics of black hole accretion, ed. M. A. Abramowicz, G. Björnsson, & J. E. Pringle (Cambridge: Cambridge Univ. Press), 50
 Abramowicz, M. A., Björnsson, G., & Pringle, J. E. 1999, *Theory of Black Hole Accretion Discs*, ed. Marek A. Abramowicz and Gunnlaugur Björnsson and James E. Pringle (Cambridge: Cambridge Univ. Press)
 Abramowicz, M. A., Jaroszyński, M., Kato, S., et al. 2010, *A&A*, 521, A15
 Bicknell, G. V. 1985, *Proceedings of the Astronomical Society of Australia*, 6, 130
 Blandford, R. D., & Znajek, R. L. 1977, *MNRAS*, 179, 433
 Blandford, R. D., & Payne, D. G. 1982, *MNRAS*, 199, 883
 Best, P. N., & Heckman, T. M. 2012, *MNRAS*, 421, 1569
 Chen, X., Abramowicz, M. A., Lasota, J.-P., Narayan, R., & Yi, I. 1995, *ApJ*, 443, L61
 De Villiers, J.-P., Hawley, J. F., & Krolik, J. H. 2003, *ApJ*, 599, 1238
 Esin, A. A., McClintock, J. E., & Narayan, R. 1997, *ApJ*, 489, 865
 Falcke, H., Körding, E., & Markoff, S. 2004, *A&A*, 414, 895
 Fanaroff, B. L., & Riley, J. M. 1974, *MNRAS*, 167, 31P
 Fender, R. P., Belloni, T. M., & Gallo, E. 2004, *MNRAS*, 355, 1105
 Ghisellini, G., & Celotti, A. 2001, *A&A*, 379, L1

- Ghisellini, G., Tavecchio, F., Foschini, L., & Ghirlanda, G. 2011, *MNRAS*, 414, 2674
- Honma, F. 1996, *PASJ*, 48, 77
- Kato, S., & Nakamura, K. E. 1998, *PASJ*, 50, 559
- Kato, S., Fukue, J., & Mineshige, S. 2008, *Black-Hole Accretion Disks — Towards a New Paradigm*, Kyoto University Press (Kyoto, Japan)
- Ledlow, M. J., & Owen, F. N. 1996, *AJ*, 112, 9
- Livio, M., Ogilvie, G. I., & Pringle, J. E. 1999, *ApJ*, 512, 100
- Maccarone, T. J., Gallo, E., & Fender, R. 2003, *MNRAS*, 345, L19
- MacDonald, D., & Thorne, K. S. 1982, *MNRAS*, 198, 345
- Manmoto, T., Kato, S., Nakamura, K. E., & Narayan, R. 2000, *ApJ*, 529, 127
- McKinney, J. C., Tchekhovskoy, A., & Blandford, R. D. 2012, *MNRAS*, 423, 3083
- Narayan, R., & Yi, I. 1994, *ApJ*, 428, L13
- Narayan, R., & Yi, I. 1995, *ApJ*, 452, 710
- Narayan, R., Kato, S., & Honma, F. 1997, *ApJ*, 476, 49
- Narayan, R., McClintock, J. E., & Yi, I. 1996, *ApJ*, 457, 821
- Narayan, R., Igumenshchev, I. V., & Abramowicz, M. A. 2003, *PASJ*, 55, L69
- Novikov, I. D., & Thorne, K. S. 1973, *Black Holes (Les Astres Occlus)*, 343
- Paczynski, B., & Wiita, P. J. 1980, *A&A*, 88, 23
- Pu, H.-Y., Hirokuni, K., Chang, H.-K. 2012, *ApJ*, 758, 113 (PHC)
- Rothstein, D. M., & Lovelace, R. V. E. 2008, *ApJ*, 677, 1221
- Sądowski, A. 2009, *ApJS*, 183, 171
- Sądowski, A., & Sikora, M. 2010, *A&A*, 517, A18
- Sądowski, A., Abramowicz, M., Bursa, M., et al. 2011, *A&A*, 527, A17
- Shakura, N. I., & Sunyaev, R. A. 1973, *A&A*, 24, 337
- Spruit, H. C., & Uzdensky, D. A. 2005, *ApJ*, 629, 960
- Takahashi, M., Nitta, S., Tatematsu, Y., & Tomimatsu, A. 1990, *ApJ*, 363, 206
- Tchekhovskoy, A., Narayan, R., & McKinney, J. C. 2011, *MNRAS*, 418, L79
- Trump, J. R., Impey, C. D., Kelly, B. C., et al. 2011, *ApJ*, 733, 60
- Urry, C. M., & Padovani, P. 1995, *PASP*, 107, 803
- Wu, Q., Cao, X., & Wang, D.-X. 2011, *ApJ*, 735, 50
- Xu, Y.-D., Cao, X., & Wu, Q. 2009, *ApJ*, 694, L107